Optogenetic stimulation of the cochlear nucleus using channelrhodopsin-2 evokes activity in the central auditory pathways

Citation: Darrow, Keith N., Michaël C.C. Slama, Elliott D. Kozin, Maryanna Owoc, Kenneth Hancock, Judith Kempfle, Albert Edge, et al. "Optogenetic Stimulation of the Cochlear Nucleus Using Channelrhodopsin-2 Evokes Activity in the Central Auditory Pathways." Brain Research 1599 (March 2015): 44–56.

As Published: http://dx.doi.org/10.1016/j.brainres.2014.11.044

Publisher: Elsevier

Persistent URL: http://hdl.handle.net/1721.1/109065

Version: Author's final manuscript: final author's manuscript post peer review, without publisher's formatting or copy editing

HHS Public Access

Author manuscript

Brain Res. Author manuscript; available in PMC 2016 May 06.

Published in final edited form as:

Brain Res. 2015 March 2; 1599: 44–56. doi:10.1016/j.brainres.2014.11.044.

Optogenetic stimulation of the cochlear nucleus using channelrhodopsin-2 evokes activity in the central auditory pathway

Keith N. Darrow[1,2], **Michaël C. C. Slama**[3,4], **Maryanna Owoc**[1], **Elliott Kozin**[3,4], **Kenneth Hancock**[3], **Judith Kempfle**[2,3], **Albert Edge**[2,3], **Stephanie Lacour**[5], **Edward Boyden**[6], **Daniel Polley**[2,3], **M. Christian Brown**[2,3], and **Daniel J. Lee**[3,4]

[1]Department of Communication Sciences and Disorders, Worcester State University, Worcester, Massachusetts [2]Eaton-Peabody Laboratories, Massachusetts Eye and Ear Infirmary, Boston, Massachusetts [3]Department of Otology and Laryngology, Harvard Medical School, Boston, Massachusetts [4]Department of Otolaryngology – Head and Neck Surgery, Massachusetts Eye and Ear Infirmary, Boston, MA [5]Laboratory for Soft Bioelectronic Interfaces, Center for Neuroprosthetics, IMT/IBI, EPFL, Switzerland [6]Departments of Brain and Cognitive Sciences and Biological Engineering, MIT Media Lab and McGovern Institute, MIT, Cambridge, Massachusetts 02139, USA

Abstract

Optogenetics has become an important research tool and is being considered as the basis for several neural prostheses. However, few studies have applied optogenetics to the auditory brainstem. This study explored whether optical activation of the cochlear nucleus (CN) elicited responses in neurons in higher centers of the auditory pathway, and it measured the evoked response to optical stimulation. Viral-mediated gene transfer was used to express channelrhodopsin-2 (ChR2) in the mouse CN. Blue light was delivered via an optical fiber placed near the surface of the infected CN and recordings were made in higher-level centers. Optical stimulation evoked excitatory multiunit spiking activity throughout the tonotopic axis of central nucleus of the inferior colliculus (IC) and the auditory cortex (Actx). The pattern and magnitude of IC activity elicited by optical stimulation was comparable to that obtained with a 50 dB SPL acoustic click stimulus. This broad pattern of activity was consistent with histological confirmation of GFP label of cell bodies and axons throughout the CN. Increasing pulse rates up to 320 Hz did not significantly affect threshold or bandwidth of the IC responses, but rates higher than 50 Hz resulted in desynchronized activity. Optical stimulation also evoked an auditory brainstem response, which had a simpler waveform than the response to acoustic stimulation. Control cases showed no responses to optical stimulation. These data suggest that optogenetic

Correspondence: Daniel J. Lee M.D., Department of Otolaryngology, Massachusetts Eye and Ear Infirmary, Harvard Medical School, 243 Charles Street, Boston, MA 02114, (617) 573 3130, Daniel_Lee@meei.harvard.edu.

Roles of authors: Designed experiments (KND, MCCS, KH, JK, AE, SL, DB, MCB, DJL), supplied expertise and reagents (KH, EB), performed experiments (KND, MCCS, EK, MO, JK), analyzed data (KND, EK, JK, DP, MCB), manuscript preparation (KND, MCCS, EK, AE, MCB, DJL).

control of central auditory neurons is feasible, but opsins with faster channel kinetics will be necessary to convey information in rates typical of many auditory signals.

Keywords

ChR2; inferior colliculus; auditory cortex; synchronization index; neural prosthesis

1. Introduction

Optogenetic control of neural pathways has been used to investigate many neural systems including memory, olfaction, motor control, and the limbic system (Boyden et al., 2005; Ayling et al., 2009; Hira et al., 2009; Rolls et al., 2011; Stortkuhl and Fiala, 2011; Huff et al., 2013; Shimano et al., 2013). Optogenetics uses viral vectors (Boyden et al., 2005) or tissue-specific promoters (Zhao et al., 2011) to deliver light-sensitive microbial opsins into neural membranes and enable the neurons to respond to optical stimulation (Boyden et al., 2005; Han and Boyden, 2007; Chow et al., 2010). Channelrhodopsin-2 (ChR2) is the most widely used opsin in neuroscience research. This molecule, when delivered to neurons of the CNS, can be activated by pulses of blue light. ChR2 has been safely expressed and stimulated, without observed immune response, *in vivo* in multiple species, including non-human primates, over a period of months to years (Zhang et al., 2006; Wang et al., 2007; Bernstein et al., 2008; Han et al., 2009; Chan et al., 2010; Chow et al., 2010).

Only a few recent studies have applied optogenetics to the auditory system. In a pioneering study of the CN, Shimano et al. (2013) introduced ChR2 into the CN neurons and demonstrated local increases in activity in response to light. In a study of the cochlea of transgenic animals expressing ChR2, stimulation of the cochlea with light activates auditory-nerve fibers and higher centers in the auditory pathway (Hernandez et al., 2014). That study proposed the idea of an auditory implant based on optogenetics, an optical cochlear implant. The cochlear implant is an auditory prosthesis implanted into the inner ear and it successfully restores hearing in terms of comprehension of speech (Moore and Shannon, 2009; Colletti et al., 2012). Another auditory prosthesis potentially amenable to the use of optogenetics is the auditory brainstem implant (ABI; (Otto et al., 1998). The ABI is an array of electrodes surgically placed on the surface of the CN, bypassing a damaged cochlea or auditory nerve in human patients who cannot benefit from a cochlear implant. The significant limitation of the ABI is that the majority of users, especially those who have had a vestibular schwannoma removed from the area, have poor speech comprehension when compared with users of the more successful cochlear implant (Colletti et al., 2012) In addition, many ABI users experience side effects (e.g. pain, facial twitching, and dizziness) from the non-specific activation of neighboring nerves affected by electric current spread. A revised design of the ABI with penetrating electrodes did not improve comprehension (Otto et al., 1998) and is no longer an option. New approaches to the ABI using optogenetics could be explored as a means to more effectively restore hearing to these deaf individuals.

In the current study, the goal was to establish the response characteristics of neurons in higher centers following stimulation of ChR2-expressing CN neurons. We chose to record in

the inferior colliculus (IC), a higher-order nucleus that receives direct projections from the CN, and from auditory cortex (Actx), which is several synapses above the CN at the highest level of the pathway. Of special interest is the limitation of optical responses to pulses of high-rates, because the ChR2 ion channel, which has sluggish kinetics (Boyden et al., 2005), is likely to limit responses to lower rates compared to that observed for acoustic stimulation. We also compared the far-field evoked response characteristics evoked by light and those evoked by sound. Given the circuitry of the CN, with a complex mix of excitatory and inhibitory neurons (Nelken and Young 1994), it is not clear what the higher-level response type will be. However, the results will be important in any future considerations of an auditory prosthesis based on optogenetics.

2. Results

2.1. Expression of ChR2 in the cochlear nucleus

Mice injected with ChR2 had ChR2-GFP immunolabeled neurons and axons throughout the three subdivisions of the CN (DCN, dorsal; PVCN, posteroventral and less label in the AVCN, anteroventral; Fig 1A). For example, there was labeling in the fusiform cell layer of DCN (Fig. 1A). There was also labeling in neuropil and axons (arrowheads in Fig 1A and insert images in Fig 1B). The anterogradely labeled axons were observed in the exit pathways of the CN (dorsal and ventral acoustic stria: (Warr, 1966; Smith et al., 1993) and in the targets of these axons, the contralateral cochlear nucleus (Cant and Gaston, 1982; Alibardi, 1998b; Brown et al., 2013a) and contralateral IC (Oliver, 1985; Schofield and Cant, 1996; Malmierca et al., 2005). Al though there was variability from animal to animal, all cases with label in the CN also had axonal label in at least 3 of the 4 brainstem locations listed above. Cases with significant label (10 or more cells or axons) in the injected CN and upstream targets were defined as ChR2+ (e.g. Fig. 1A), whereas cases with no label in the CN were defined as ChR2− (e.g. Fig. 1C). For the most part, however, the density of extracellular immunofluorescence hindered identification of discrete cell types in the CN. In total, 18 of the 27 cases were ChR2+, and the remaining 9 were ChR2− (these included the 2 sham surgery and 1 control mice). In two ChR2+ cases the cochlea and auditory nerve was examined for retrograde label of the virus; none was detected.

2.2. Responses of higher centers to optogenetic activation of the cochlear nucleus

Optical stimulation of the CN in ChR2+ cases evoked spiking activity in the contralateral IC. The response pattern of a typical recording to a light pulse is provided in Figure 2. A dot raster plot from a single electrode demonstrated the timed pattern of response to pulses of different intensities (Fig. 2A). At low intensities, only spontaneous activity was observed, whereas at higher intensities, there was a clear response within the first 10 ms following stimulus onset. The rate-intensity function for the same electrode was a well fit by a sigmoidal function with a threshold of 6 dB re: 1 W/m^2 (Fig 2B). The threshold across 16 electrodes (Fig. 2D) averaged 9.2 dB re: 1 W/m^2 (STD was 1.5 and the SEM was 0.4), with the lowest activation threshold of 6 dB re: 1 W/m^2 recorded from the electrode with the highest firing rates (electrode #8, Fig. 2D). The light-driven response increased with level to quickly saturate at a stimulation level between 15–20 dB re: 1 W/m^2. In ChR2+ cases, when the light intensity was sufficient to elicit a response in IC, an increasing monotonic

relationship between firing rate and pulse rate was observed (Fig 2E). The spatial pattern of optically driven multiunit responses was broad in most cases. Here, it was observed on all 16 electrodes (Fig. 2C, activation index, 16), which spanned the tonotopic axis of the IC. Across all Chr2+ cases, the mean activation width was 11.8 (SD 5.7), whereas it was only 0.2 (SD 0.4) in ChR2− and control mice.

To control for any potential optophonic or electrical artifact, multiunit activity in ChR2+ cases was measured with the laser off, laser pointing away from the animal, and the laser in the ear canal (to assess whether laser stimulation produced an acoustic artifact). No responses were recorded in these control experiments. In addition, no optical responses were detected in sham or control mice or in a ChR2− mouse.

In mammals, the auditory system is capable of synchronizing to temporal aspects of incoming stimuli, including pure-tone and amplitude modulated tones, up to 4000 Hz (Liberman, 1978; Rhode and Greenberg, 1994). ChR2+ mice also showed synchrony, with peristimulus time histograms (Fig 3A) demonstrating a clear time-locked increase in activity at suprathreshold levels. The synchronization index (SI), a measure of synchronization to the stimulus pulse-rate, of the response measured from an electrode in the 20 kHz region of the IC was well fit with a sigmoidal function having a synchronization threshold near 10 dB re: 1 W/m^2 and a saturation point near 25 dB re: 1 W/m^2 (Fig 3B). The SI for all 16 electrodes spanning the IC was significant (Fig 3C & 3D). SI threshold ranged between 10–15 dB re: 1 W/m^2 (mean threshold of 12.7dB with STD of 1.3 and SEM of 0.3) with the lowest threshold equivalent to the electrode with the lowest rate threshold. No synchronization was detected when the laser was off or not directly on the surface of the DCN.

In Chr2+ cases, the SI index decreased for pulse rates above 33 Hz (Fig 3E), as is expected from the limits of ChR2 (Boyden et al., 2005; Ishizuka et al., 2006; Lin et al., 2009). The SI for all ChR2+ cases was much lower for pulse rates of 320 Hz than for 5 Hz (Fig 4A, right). Maximal firing up to 600 sp/s was found at the higher pulse rate but was somewhat lower at the low rate (Fig 4A, left). Firing rate thresholds, though, were not significantly different, but synchronization index threshold was lower for low pulse rates (Fig 4B). Activation width was not significantly different between the two pulse rates for both firing rate and synchronization (data now shown).

Responses to light stimulation of the CN were also found in a higher center of the auditory pathway, the auditory cortex (Actx) (n=2 mice). There was broad activation across electrodes (Fig. 5), which were placed along the tonotopic axis (caudal-rostral dimension). The activation index in this case was again 16 (all 16 electrodes were responsive). Thresholds were 10 – 20 dB re: 1W/cm^2 range (Fig. 5), similar to thresholds for IC responses. These findings suggest that optogenetic stimulation of the CN evokes activity in the entire central auditory pathway.

2.3. Comparing Acoustic, Electric and Optical stimulation of Auditory Pathway

Optical stimulation and auditory stimulation both resulted in broad response profiles in the IC (Fig 6). Optical stimulation (Fig. 6A, top) and acoustic stimulation with a click (Fig 6B top panel) produced approximately the same firing rates. A comparison of SI to optical or

acoustic stimulation also revealed a common pattern across modalities (Fig 6A, B bottom panels), however SI values in response to optical stimulation were always less (note differences in color scales). Overall, the spatial pattern of light-evoked optogenetic response is similar to that of the response evoked by a broadband acoustic stimulus (i.e. broad activation with monotonic increases in firing rate and SI as a function of stimulus intensity); however its synchrony is distinctly lower.

Optogenetic stimulation produced an optically evoked ABR (Fig 7). In each of 5 ChR2+ cases examined at pulse rates of 7 – 47 pulses/s, a response was observed with either a single waveform peak (Fig 7B) or a multi-peak waveform. No optical response was elicited in the two sham surgical cases or in an age-matched control CBA/CaJ mouse. The waveform of this oABR differed from that of the acoustic ABR, which had at least 5 waveform peaks (Fig. 7A). Electric stimulation produced a characteristic waveform with multiple positive and negative peaks within the first 7 ms (Fig 7C). Each of the three different stimulation modalities (acoustic, optical and electrical) produced multi-peak waveforms that were significantly different in size and latency of peaks. However, when output (μV) was normalized for each modality and the peak growth was analyzed, each of the I–O curves had a similar shape (Fig. 7D).

3. Discussion

Overall, this study demonstrates that light stimuli presented to the CN after viral infection of ChR2 activates major centers (IC and Actx) in the auditory pathway. These optogenetic results are more encouraging than those obtained using infrared neural stimulation, which does not produce responses in the CN (Verma et al., 2014).

3.1. Cell types in the CN infected by ChR2

The CN contains a variety of cell types and projections (Osen and Roth, 1969; Willard and Ryugo, 1983; Hackney et al., 1990) and our data suggest that a range of these types can be infected. For example, labeling was observed in all three CN subdivisions, and since each contains distinct types of neurons, there are at least several types of neurons that are ChR2 positive. In the DCN, label was observed in the fusiform cell layer, and axons likely to be from fusiform cells were observed in the dorsal acoustic stria and IC. Labeling of axons in the contralateral CN shows that commissural pathways can be labeled, and these originate in a subset of CN multipolar cells (Cant and Gaston, 1982; Shore et al., 1992; Brown et al., 2013a). Labeling of axons in the ventral acoustic stria must originate in neurons of the PVCN and AVCN and these could be from bushy and/or multipolar cells. The use of a CAG promoter may be responsible for labeling in diverse types of CN cells. Present results suggesting that ChR2 is transported mainly in the anterograde direction are similar to previous studies (Chamberlin et al., 1998; Shimano et al., 2013). It is not clear to what extent our responses arise from stimulation of neuronal cell bodies vs. axons since both are labeled.

It is also not clear to what extent our responses are affected by inhibitory neurons, which are present at the level of the CN. For example, commissural multipolar cells, whose axons were labeled here, consist of both excitatory and inhibitory subclasses (Cant and Gaston, 1982;

Shore et al., 1992; Brown et al., 2013a). In the DCN, which is the most superficial part of the CN directly beneath the optical fiber in our experiments, there are both excitatory and inhibitory neurons, an the neural output is shaped by the characteristics of each (Nelken and Young, 1994). We did not observe inhibitory responses at the level of the IC, but our simple paradigm could be modified in ways to search for these, such as optical stimulation interleaved with presentation of a tone.

3.2. Optical stimulation of the ChR2+ CN produces a broad spatial pattern of activation

The responses measured in the IC were broad and spanned much of the entire tonotopic (dorsal-ventral) axis of the central nucleus. They were in general character much like the response profile evoked by an acoustic click. Similarly, responses to light in Actx were broad along its tonotopic axis. The simplest explanation for the broad pattern of activity was the broad expression pattern of ChR2 across the CN. This, coupled with the fact that a wide-diameter optical fiber was used (400 μm, which spans much of the mouse DCN), suggests that optogenetic excitation across the CN was conveyed to the higher centers of the auditory pathway. Fibers of smaller dimensions, or expression of ChR2 in limited areas, will be necessary to demonstrate frequency-specific activation in the CN.

3.3. Synchrony of optogenetic responses falls off at moderate pulse rates

The responses in IC were synchronized to pulse rates up to approximately 50 pulses/s, typical of ChR2 kinetics (Boyden et al., 2005; Ishizuka et al., 2006; Lin et al., 2009). However, for an auditory prosthesis, increased synchrony at higher rates may be required. In cochlear implant users, it is estimated that the user is capable of detecting meaningful pitch percepts by modifying stimulation rates up to 300 Hz (Eddington et al., 1978; Tong and Clark, 1985; Zeng, 2002). Our findings demonstrate that ChR2, in its current state, does not meet the criteria for this type of synchronous activity. Future generations of opsins (e.g. ChIEF, ChETA and Chronos) may be more appropriate to optimally carry auditory information by synchronizing to high-rate pulses (Lin et al., 2009; Gunaydin et al., 2010; Klapoetke et al., 2014).

Optical stimulation of the CN was synchronized enough, however, to generate an auditory brainstem response, the oABR. The ABR evoked by sound is a multi-peaked waveform that represents ascending neural activity from within the auditory nerve and brainstem (Melcher and Kiang, 1996). Like the oABR from cochlear stimulation (Hernandez et al., 2014), the oABR from CN stimulation had a waveform that was had fewer peaks and was broader compared to that from acoustic stimulation. In addition to directly stimulating the CN neurons and thus by-passing the auditory nerve response, the oABR is also influenced by the slow kinetics of the ChR2 channel (Boyden et al., 2005), which may decrease the temporal synchrony of the response generators compared with the synchrony associated with sound responses. In addition, the acoustic ABR's main contributions are from CN bushy cells (Melcher and Kiang, 1996), but it is not clear whether this is true for the oABR.

3.4. An eventual auditory neuroprosthesis based on light?

Our new results suggest that an optogenetic prosthesis could provide a way of eliciting auditory percepts for those individuals lacking auditory-nerve function, who are currently

obliged to accept the current version of the ABI and its inherent limitations. In our experiments, the neurons expressing ChR2 respond to light applied to the surface of the CN, and they activate much of the central auditory pathway and should thus evoke hearing sensations. Light of the wavelength used here (473 nm) penetrates through water at least several millimeters (Richter and Tan, 2014), and it likely penetrates throughout the entire extent of the thin CN of the mouse and may penetrate to the deeper areas of the human CN (Moore and Osen, 1979; Rosahl and Rosahl, 2013). Surface light, compared to the surface electrical stimulation in the conventional ABI (McCreery et al., 2007), has the potential to convey a more focused stimulation to deep neural tissue. More focused stimulation might avoid the side effects (e.g. pain, facial twitching, and dizziness) that are common for some electrodes of the conventional ABI array. Although the present study did not show this for the CN, optical stimulation of the cochlea excites narrower regions of the IC than monopolar electrical stimulation (Hernandez et al., 2014). Thus, an optical auditory prosthesis could offer finer frequency selectivity, since best frequency is mapped to spatial position in most central auditory nuclei. To take advantage of this characteristic, an optogenetic ABI would require a number of independent stimulation channels for transmitting the spectrum of the acoustic signal. Our results show, though, that an opsin providing higher synchrony will be needed to convey the rapid modulations in the speech signal. And finally, it remains to be seen whether a new type of ABI can circumvent the challenge of speech coding in a CN that has been damaged by the presence of a tumor or its removal from the 8th cranial nerve (Colletti et al., 2012).

4. Experimental Procedure

4.1. Surgical Procedures and Infection of AAV2/8-ChR2 to the CN

All experimental procedures on CBA/CaJ mice were performed in accordance with the National Institutes of Health guidelines for the care and use of laboratory animals as well as approved animal care and use protocols at the Massachusetts Eye & Ear Infirmary, Boston, MA.

4.2. Surgical Procedures and Infection of AAV2/8-ChR2

Normal hearing CBA/CaJ mice (n=27) were aged 8–12 weeks, weighing 18–24 g, and of either sex. Following anesthesia (xylazine 20 mg/kg, given intraperitoneally [i.p.] and ketamine 100 mg/kg, i.p.) the mouse was held in a Kopf (Tujunga, CA) small-animal stereotaxic apparatus by snout clamp. The skin overlaying the skull was slit and a craniotomy of the left posterior skull surface was performed using rongeurs. Partial cerebellar aspiration (of the left hemisphere) exposed the dorsal surface of the brainstem with the ampulla of the semicircular canal as a general landmark. The left dorsal cochlear nucleus (DCN) was identified by brainstem surface landmarks (there was no attempt to visualize the auditory nerve as it enters the CN ventrally. Direct exposure of the DCN, rather than stereotaxic injection, was used to minimize the chances of missing the desired injection site. Pressure injections of between 1.0–2.0 μl of adeno-associated virus with channelrhodopsin-2 (AAV2.8-ChR2 fused with GFP and CAG promoter; (Alexopoulou et al., 2008) for 2–4 minutes were made into the CN using a 10 μl Hamilton (Reno, NV) syringe in 24 mice. Immediately following injection, the incision was closed and the scalp

was sutured. Four additional mice were used as either 'sham' or control cases. Sham mice (n=2) underwent the exact surgical protocol as injected mice, including insertion of an empty Hamilton syringe in to the brainstem for 2–3 minutes. Control mice (n=2) had no history of manipulation.

After a 3–4 week survival time to allow for expression of the ChR2, the mice were prepared for acute surgery to characterize responses to optical stimulation. Initial anesthesia was as above with 60–80 mg/kg ketamine supplements as necessary. Using a scalpel, the injected region was re-exposed (for optical stimulation) and a craniotomy was made over the right inferior colliculus and/or the right auditory cortex (for recordings). The brain surface was covered with high-viscosity silicon oil. During the course of physiological recordings, the core body temperature of the animal was maintained at 36.8°C with a homeothermic blanket system. After all recordings were made, the animal was sacrificed with an overdose of ketamine, brainstems were extracted and post-fixed for 2 hours, cryoprotected in 30% sucrose for 24–48 hours, frozen, and cut on a cryostat and coronal sections were cut at 60 μm.

Brainstem tissue was processed to enhance visualization of ChR2-GFP. Before the staining procedure, sections were allowed to dry at room temperature and then rehydrated in PBS for 10 min. After washing with PBS, tissue was permeabilized and blocked with blocking solution (0.3% Triton X-100, 15% heat inactivated goat or donkey serum in PBS) for 1 h. Primary antibody was diluted (0.1% Triton X-100, and 10% heat inactivated goat or donkey serum in PBS) and applied to the tissue overnight at 4° C. Antibody dilutions were: 1:400 for monoclonal mouse anti-B-Tubulin (Covance), and 1:800 for polyclonal rabbit anti-GFP (Invitrogen). Secondary antibodies (Alexafluor 488- and 568- conjugated; Invitrogen) were used to detect primary antibodies. Visualization of nuclei was performed with 4,6-diamidino-2-phenylindole (DAPI), (Vector Laboratories). Staining was analyzed with epifluorescence microscopy (Axioskop2 Mot Axiocam, Zeiss) and confocal microscopy (TCD, Leica).

Using a fluorescence microscope, a histological analysis of ChR2-GFP label in the brainstem was performed in each case 3–4 weeks after injection of viral mediated ChR2 (the observer was blind as to case number and surgical history). The presence or absence of GFP labeled cells in CN and axons in CN exit pathways and targets were noted.

4.3. Physiological Data Collection

4.3.1. Stimuli—Optical stimuli were produced by a laser (BL473T-100FC, Shanghai Laser & Optics Century Co.), led through an optical fiber (400 μm diameter) with the tip directly contacting the exposed surface of the DCN. Blue light (473 nm) pulses of 1 ms duration presented continuously at 5 pulses/sec unless otherwise indicated. The number of pulse presentations was typically 80, but varied from 40 to 120. For the subset of experiments characterizing the effect of pulse rate, pseudorandomized 500 ms pulse trains, followed by 500 ms with no stimulation, were presented with pulse rates ranging from 5–320 Hz. For both protocols, light intensity was varied between −15.4 and 29.1 dB re: 1 W/cm^2, which adequately captured the range of firing rate responses from threshold to saturation. The laser was calibrated by positioning the optical fiber 2 mm from a high-sensitivity thermopile

sensor (Coherent PS19Q) connected to a power meter (Coherent LabMax-TOP). The voltage command parameters were systematically varied, and the measured power was divided by the cross-sectional area of the fiber and by the pulse rate to get the radiant exposure in mJ/cm^2.

4.3.2. Multiunit recordings—Multiunit recordings were made from the central nucleus of the IC or Actx using either a 16-channel linear silicon probe or a 4×4 shank array, respectively (both with 177 μm^2 contact area, 50 μm contact separation, NeuroNexus Technologies). Final adjustments in position of the recording electrodes were made to obtain a complete tonotopic mapping across the recording channels (Malmierca et al., 1993; Guo et al., 2012) from 11.3 to 45.25 kHz in 0.5 octave steps and from 0–80 dB in 10 dB steps, using 20 ms duration tone bursts with a repetition rate of 10 bursts/s.

4.3.3. Spike detection—Voltage waveforms of multiunit activity were measured with the 16-channel recording electrodes, amplified, and recorded to disk. To remove slow fluctuations in the signal due to movement or other slow artifacts, the mean waveform across the 16 electrode channels was computed and subtracted from the individual channel waveforms. Additional electrical and physiological noise was further removed by filtering the resulting waveforms between 500 and 3000 Hz with 5-point Butterworth filters. Spikes were defined as waveform segment that had values greater than 4 times (a factor determined empirically) the background noise level after filtering. For pulse rates of 5 Hz, the background noise level was measured as the median value of the filtered waveform between 12 ms post-stimulus onset and the onset of the following pulse (optically evoked spiking was never observed at a time longer than 12 ms post-stimulus onset). For pulse rates higher than 5 Hz, the background noise level was defined as the median value of the filtered waveform during the period between pulse trains.

4.3.4. Firing rate and activation thresholds—To compute average firing rate, spike count was determined in a set analysis window and divided by window duration. For 5 Hz pulse trains, the analysis window was 1–12 ms post-stimulus onset. For higher pulse rates, the analysis was completed during the 500 ms stimulation period. For each electrode, firing rate was plotted as a function of light intensity and the resulting rate/intensity function (RIF) was fitted with a sigmoid curve. Spontaneous firing rate was computed for each electrode from the OFF portion of the response (e.g. the 12–200 ms window for pulses at 5 Hz, or the 500 ms OFF region for pulses at higher rates). Evoked firing rates were compared between the analysis window and the spontaneous period across various pulse rates and pulse amplitudes with a paired t-test. For each electrode number, the logarithm of the p-values was plotted as a function of light intensity and fitted with a sigmoid curve. Activation threshold was determined as the light intensity at which the fitted log-p-value/intensity function became smaller than 0.01. Activation width was defined as the number of electrodes that crossed activation threshold.

4.3.5. Synchronization index and synchronization thresholds—To investigate temporal properties of laser-evoked spiking we computed the synchronization index (SI; (Goldberg and Brown, 1969), during a response window of 1–12 ms post-stimulus onset.

The SI varies between 0 (no synchronization) and 1 (all spikes occurring exactly at the same phase of the stimulus period). For each electrode, SI was plotted as a function of light intensity and fitted with a sigmoid curve. A Rayleigh test of uniformity was used to assess the significance of the computed SI (Mardia and Jupp, 1999.). Similarly to our determination of activation threshold, the logarithm of the p-values obtained with the Rayleigh tests was plotted against light intensity and fitted with a sigmoid curve. Synchronization threshold was determined as the light intensity at which the fitted log-p-value/intensity function crossed 0.01.

4.3.6. Auditory Brainstem Response (ABR) and Distortion Product Otoacoustic Emissions (DPOAE) tests—ABR measurements were recorded under anesthesia with needle electrodes inserted in the vertex and pinna, and with a ground near the tail. ABRs were evoked in response to acoustic stimulation (5-ms tone pips at 16 kHz or click), CN electrical stimulation (biphasic bipolar pulses, 0–0.4mA, 7–27Hz) or CN optical stimulation (1ms, 7–27Hz pulse rate). The electric stimulation was delivered to the surface of the CN using a pair of stainless steel wires insulated except at the tip (200 μm diam.; impedance 0.1–0.5 MΩ) and was presented through a stimulus isolator (Model 2200, A-M Systems, Carlsborg, WA). For ABR recordings, evoked responses were amplified, filtered and averaged. DPOAE tests were used to determine any changes in cochlear function following virus injections. 2f1–f2 emissions were recorded in response to primary tones: f1 and f2, with f2/f1 = 1.2 and f2 level 10 dB < f1 level, with f2 at 8.0, 11.3, 22.6, 32.0, and 45.25kHz. In all cases, the DPOAEs and tone-pip ABR thresholds were within normal limits for CBA/CaJ mice at 12–16 weeks old (data not shown).

Acknowledgments

Preliminary results of this study were presented at the Association for Research in Otolaryngology Midwinter Meeting, February 2013. This work was supported by a Fondation Bertarelli grant (D.J.L and S.L), a MED-EL grant (D.J.L), and a National Institutes of Health Grants DC01089 (M.C.B.) and DC012894 (D.P.).

References

Alexopoulou AN, Couchman JR, Whiteford JR. The CMV early enhancer/chicken beta actin (CAG) promoter can be used to drive transgene expression during the differentiation of murine embryonic stem cells into vascular progenitors. BMC cell biology. 2008; 9:2. [PubMed: 18190688]

Alibardi I. Ultrastructural and immunocytochemical characterization of commissural neurons in the ventral cochlear nucleus of the rat. Ann Anat. 1998b; 180:427–438. [PubMed: 9795693]

Ayling OG, Harrison TC, Boyd JD, Goroshkov A, Murphy TH. Automated light-based mapping of motor cortex by photoactivation of channelrhodopsin-2 transgenic mice. Nat Methods. 2009; 6:219–224. [PubMed: 19219033]

Bernstein JG, Han X, Henninger MA, Ko EY, Qian X, Franzesi GT, McConnell JP, Stern P, Desimone R, Boyden ES. Prosthetic systems for therapeutic optical activation and silencing of genetically-targeted neurons. Proc Soc Photo Opt Instrum Eng. 2008; 6854:68540H.

Boyden ES, Zhang F, Bamberg E, Nagel G, Deisseroth K. Millisecond-timescale, genetically targeted optical control of neural activity. Nat Neurosci. 2005; 8:1263–1268. [PubMed: 16116447]

Brown MC, Drottar M, Benson TE, Darrow KN. Commissural axons of the mouse cochlear nucleus. J Comp Neurol. 2013a; 521:1683–1696. [PubMed: 23124982]

Cant NB, Gaston KC. Pathways connecting the right and left cochlear nuclei. J Comp Neurol. 1982; 212:313–326. [PubMed: 6185548]

Chamberlin NL, Du B, de Lacalle S, Saper CB. Recombinant adeno-associated virus vector: use for transgene expression and anterograde tract tracing in the CNS. Brain Res. 1998; 793:169–175. [PubMed: 9630611]

Chan S, Bernstein J, Boyden E. Scalable fluidic injector arrays for viral targeting of intact 3-D brain circuits. J Vis Exp. 2010

Chow BY, Han X, Dobry AS, Qian X, Chuong AS, Li M, Henninger MA, Belfort GM, Lin Y, Monahan PE, Boyden ES. High-performance genetically targetable optical neural silencing by light-driven proton pumps. Nature. 2010; 463:98–102. [PubMed: 20054397]

Colletti L, Shannon R, Colletti V. Auditory brainstem implants for neurofibromatosis type 2. Curr Opin Otolaryngol Head Neck Surg. 2012; 20:353–357. [PubMed: 22886036]

Eddington DK, Dobelle WH, Brackmann DE, Mladejovsky MG, Parkin JL. Auditory prostheses research with multiple channel intracochlear stimulation in man. Ann Otol Rhinol Laryngol. 1978; 87:1–39. [PubMed: 736424]

Goldberg JM, Brown PB. Response of binaural neurons of dog superior olivary complex to dichotic tonal stimuli: Some physiological mechanisms of sound localization. J Neurophysiol. 1969; 32:613–636. [PubMed: 5810617]

Gunaydin LA, Yizhar O, Berndt A, Sohal VS, Deisseroth K, Hegemann P. Ultrafast optogenetic control. Nat Neurosci. 2010; 13:387–392. [PubMed: 20081849]

Guo W, Chambers AR, Darrow KN, Hancock KE, Shinn-Cunningham BG, Polley DB. Robustness of cortical topography across fields, laminae, anesthetic states, and neurophysiological signal types. The Journal of neuroscience: the official journal of the Society for Neuroscience. 2012; 32:9159–9172. [PubMed: 22764225]

Hackney CM, Osen KK, Kolston J. Anatomy of the cochlear nuclear complex of the guinea pig. Anat Embryol. 1990; 182:123–149. [PubMed: 2244686]

Han X, Boyden ES. Multiple-color optical activation, silencing, and desynchronization of neural activity, with single-spike temporal resolution. PloS one. 2007; 2:e299. [PubMed: 17375185]

Han X, Qian X, Bernstein JG, Zhou HH, Franzesi GT, Stern P, Bronson RT, Graybiel AM, Desimone R, Boyden ES. Millisecond-timescale optical control of neural dynamics in the nonhuman primate brain. Neuron. 2009; 62:191–198. [PubMed: 19409264]

Hernandez VH, Gehrt A, Reuter K, Jing Z, Jeschke M, Mendoza Schulz A, Hoch G, Bartels M, Vogt G, Garnham CW, Yawo H, Fukazawa Y, Augustine GJ, Bamberg E, Kugler S, Salditt T, de Hoz L, Strenzke N, Moser T. Optogenetic stimulation of the auditory pathway. The Journal of clinical investigation. 2014; 124:1114–1129. [PubMed: 24509078]

Hira R, Honkura N, Noguchi J, Maruyama Y, Augustine GJ, Kasai H, Matsuzaki M. Transcranial optogenetic stimulation for functional mapping of the motor cortex. J Neurosci Methods. 2009; 179:258–263. [PubMed: 19428535]

Huff ML, Miller RL, Deisseroth K, Moorman DE, LaLumiere RT. Posttraining optogenetic manipulations of basolateral amygdala activity modulate consolidation of inhibitory avoidance memory in rats. Proceedings of the National Academy of Sciences of the United States of America. 2013; 110:3597–3602. [PubMed: 23401523]

Ishizuka T, Kakuda M, Araki R, Yawo H. Kinetic evaluation of photosensitivity in genetically engineered neurons expressing green algae light-gated channels. Neurosci Res. 2006; 54:85–94. [PubMed: 16298005]

Klapoetke NC, et al. Independent optical excitation of distinct neural populations. Nat Methods. 2014; 11:338–346. [PubMed: 24509633]

Liberman MC. Auditory-nerve responses from cats raised in a low-noise chamber. J Acoust Soc Am. 1978; 63:442–455. [PubMed: 670542]

Lin JY, Lin MZ, Steinbach P, Tsien RY. Characterization of engineered channelrhodopsin variants with improved properties and kinetics. Biophys J. 2009; 96:1803–1814. [PubMed: 19254539]

Malmierca MS, Saint Marie RL, Merchan MA, Oliver DL. Laminar inputs from dorsal cochlear nucleus and ventral cochlear nucleus to the central nucleus of the inferior colliculus: Two patterns of convergence. Neurosci. 2005; 136:883–894.

Malmierca MS, Blackstad TW, Osen KK, Karagulle T, Molowny RL. The central nucleus of the inferior colliculus in rat: A Golgi and computer reconstruction study of neuronal and laminar structure. J Comp Neurol. 1993; 333:1–27. [PubMed: 7688006]

Mardia, KV.; Jupp, PE. Directional Statistics. New York: Wiley; 1999.

McCreery D, Lossinsky A, Pikov V. Performance of multisite silicon microprobes implanted chronically in the ventral cochlear nucleus of the cat. IEEE transactions on bio-medical engineering. 2007; 54:1042–1052. [PubMed: 17554823]

Melcher JR, Kiang NYS. Generators of the brainstem auditory evoked potential in cat III: Identified cell populations. Hearing Res. 1996; 93:52–71.

Moore DR, Shannon RV. Beyond cochlear implants: awakening the deafened brain. Nat Neurosci. 2009; 12:686–691. [PubMed: 19471266]

Moore JK, Osen KK. The cochlear nuclei in man. Am J Anatomy. 1979; 154:393–418.

Nelken I, Young ED. Two separate inhibitory mechanisms shape the responses of dorsal cochlear nucleus type IV units to narrowband and wideband stimuli. J Neurophysiol. 1994; 71:2446–2462. [PubMed: 7931527]

Oliver DL. Quantitative analyses of axonal endings in the central nucleus of the inferior colliculus and distribution of 3H-labelling after injections in the dorsal cochlear nucleus. J Comp Neurol. 1985; 237:343–359. [PubMed: 4044892]

Osen KK, Roth K. Histochemical localization of cholinesterases in the cochlear nuclei of the cat, with notes on the origin of acetylcholinesterase-positive afferents and the superior olive. Brain Res. 1969; 16:165–185. [PubMed: 5348847]

Otto SR, Shannon RV, Brackmann DE, Hitselberger WE, Staller S, Menapace C. The multichannel auditory brain stem implant: Performance in twenty patients. Otolaryngol - Head & Neck Surgery. 1998; 118:291–303.

Rhode WS, Greenberg S. Encoding of amplitude modulation in the cochlear nucleus of the cat. J Neurophysiol. 1994; 71:1797–1825. [PubMed: 8064349]

Richter CP, Tan X. Photons and neurons. Hearing research. 2014

Rolls A, Colas D, Adamantidis A, Carter M, Lanre-Amos T, Heller HC, de Lecea L. Optogenetic disruption of sleep continuity impairs memory consolidation. Proceedings of the National Academy of Sciences of the United States of America. 2011; 108:13305–13310. [PubMed: 21788501]

Rosahl SK, Rosahl S. No easy target: Anatomic constraints of electrodes interfacing the human cochlear nucleus. Neurosurgery. 2013; 72:58–64. S. Opperative. [PubMed: 22895407]

Schofield BR, Cant NB. Projections from the ventral cochlear nucleus to the inferior colliculus and the contralateral cochlear nucleus in guinea pigs. Hearing Res. 1996; 102:1–14.

Shimano T, Fyk-Kolodziej B, Mirza N, Asako M, Tomoda K, Bledsoe S, Pan ZH, Molitor S, Holt AG. Assessment of the AAV-mediated expression of channelrhodopsin-2 and halorhodopsin in brainstem neurons mediating auditory signaling. Brain Res. 2013; 1511:138–152. [PubMed: 23088961]

Shore SE, Helfert RH, Bledsoe SC, Altschuler RA, Godfrey DA. Connections between the cochlear nuclei in guinea pig. Hearing Res. 1992; 62:16–26.

Smith PH, Joris PX, Yin TCT. Projections of physiologically characterized spherical bushy cell axons from the cochlear nucleus of the cat: Evidence for delay lines to the medial superior olive. J Comp Neurol. 1993; 331:245–260. [PubMed: 8509501]

Stortkuhl KF, Fiala A. The Smell of Blue Light: A New Approach toward Understanding an Olfactory Neuronal Network. Front Neurosci. 2011; 5:72. [PubMed: 21647413]

Tong YC, Clark GM. Absolute identification of electric pulse rates and electrode positions by cochlear implant patients. J Acoust Soc Am. 1985; 77:1881–1888. [PubMed: 3839004]

Verma RU, Guex AA, Hancock KE, Durakovic N, McKay CM, Slama MC, Brown MC, Lee DJ. Auditory responses to electric and infrared neural stimulation of the rat cochlear nucleus. Hearing research. 2014; 310:69–75. [PubMed: 24508368]

Wang H, Peca J, Matsuzaki M, Matsuzaki K, Noguchi J, Qiu L, Wang D, Zhang F, Boyden E, Deisseroth K, Kasai H, Hall WC, Feng G, Augustine GJ. High-speed mapping of synaptic connectivity using photostimulation in Channelrhodopsin-2 transgenic mice. Proceedings of the

National Academy of Sciences of the United States of America. 2007; 104:8143–8148. [PubMed: 17483470]

Warr WB. Fiber degeneration following lesions in the anterior ventral cochlear nucleus of the cat. Exp Neurol. 1966; 14:453–474. [PubMed: 4378200]

Willard, FH.; Ryugo, DK. Anatomy of the central auditory system. In: Willott, JF., editor. The Auditory Psychobiology of the Mouse. Springfield, IL: C.C. Thomas; 1983. p. 201-304.

Zeng FG. Temporal pitch in electric hearing. Hearing research. 2002; 174:101–106. [PubMed: 12433401]

Zhang F, Wang LP, Boyden ES, Deisseroth K. Channelrhodopsin-2 and optical control of excitable cells. Nat Methods. 2006; 3:785–792. [PubMed: 16990810]

Zhao S, Ting JT, Atallah HE, Qiu L, Tan J, Gloss B, Augustine GJ, Deisseroth K, Luo M, Graybiel A, Feng G. Cell type-specific channelshodopsin-2 transgneic mice for optogenetic dissection of neural circuitry function. Nat Meth. 2011; 8:745–752.

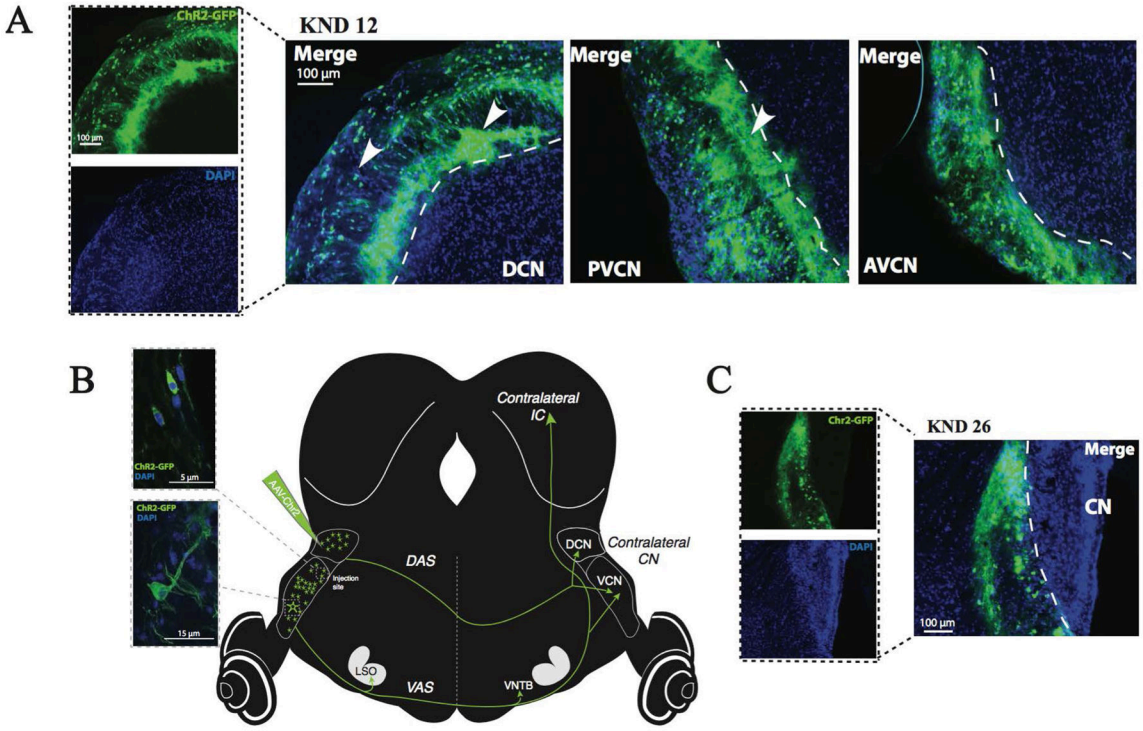

Figure 1.

Histological localization of ChR2-GFP. A) Fluorescent images of ChR2-GFP (top, left) and DAPI staining to indicate neurons (bottom, left) are merged into a composite view in the DCN. Other merged images indicate composites of staining in the PVCN and AVCN (all from case KND 12). Arrowheads indicate immunofluorescence label in fusiform cell layer and extracellular label in deeper DCN that obscures cell-type identification. B) High-magnification confocal images (merged DAPI and ChR2-GFP staining) of CN cell bodies. Schematic illustrates positions of ChR2 expression in cell bodies of the CN and in anterogradely labeled axons in the dorsal and ventral acoustic stria (DAS and VAS), the contralateral CN, and contralateral IC. C) Fluorescent images of a ChR2- case (e.g. KND 26) in which the expression pattern is observed outside the CN (just medial to it). In this and other ChR2- cases, no neuronal labeling of auditory brainstem structures was observed.

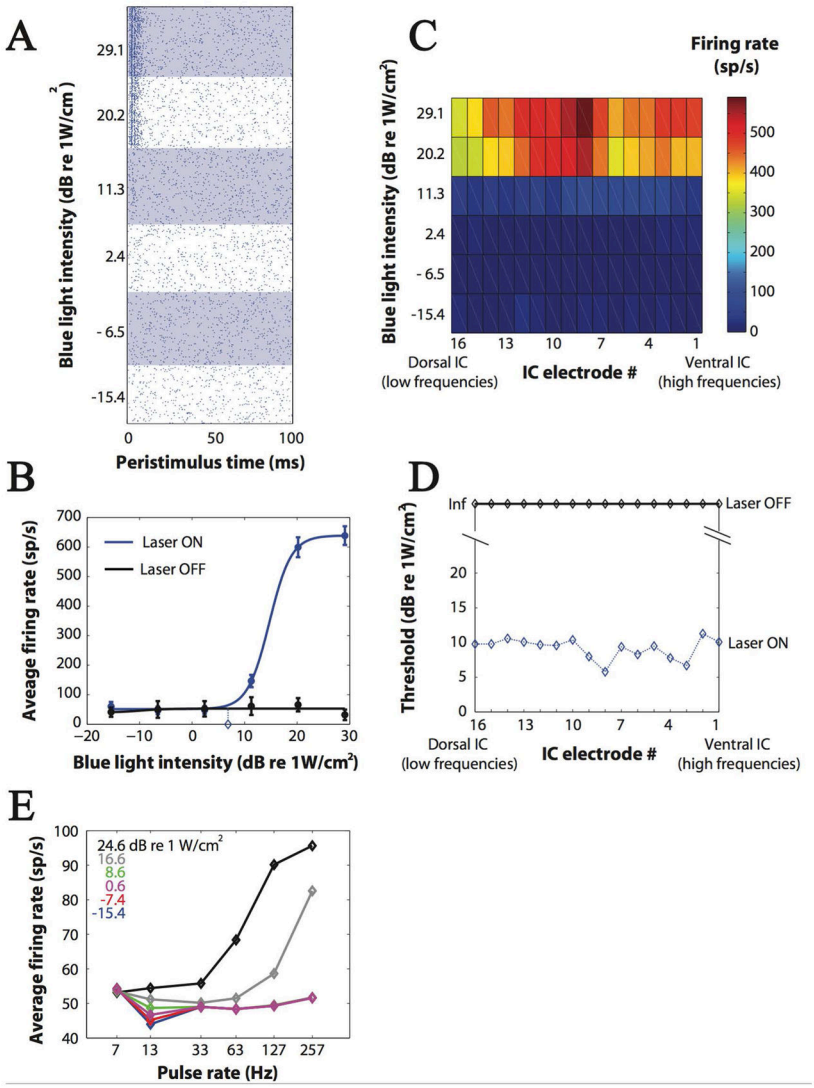

Figure 2.

Responses to light in IC in ChR2+ cases (A–D: KND 23; E: KND37). A) Dot rasters at increasing light intensities from a single electrode in the IC (#8, with best response to sound frequency of 20 kHz). Each dot represents a multiunit action potential and there were 120 presentations for each light intensity. At low intensities, there is only spontaneous activity, whereas at higher intensities, there was driven activity in the first 10 ms following stimulus onset. B) Average firing rate between 1 and 12 ms in this electrode as a function of light intensity (blue dots, with error bars indicating ± 2 standard errors; solid blue line: sigmoidal fit). The threshold (blue diamond) was near 6 dB re: 1W/cm^2 and the saturation occurred near 20 dB re: 1W/cm^2. Black line and symbols show little response when the laser was off. C) Firing rate across all 16 recording electrodes showing the abrupt threshold above which there is broad activation. The baseline firing rate in each electrode was subtracted to facilitate comparison across electrodes. D) Thresholds were similar across all recording electrodes (about 10 dB re: 1W/cm^2). Response window was 1 and 12 ms post-stimulus. E) Effect of pulse rate on firing rate across different light intensities Stimuli were 500 ms pulse

trains and response window was the entire 500 ms (electrode #14, with best response to sound frequency of 16 kHz). Firing rate increased as a function of light pulse rate, consistent with the increased stimulation energy per cycle.

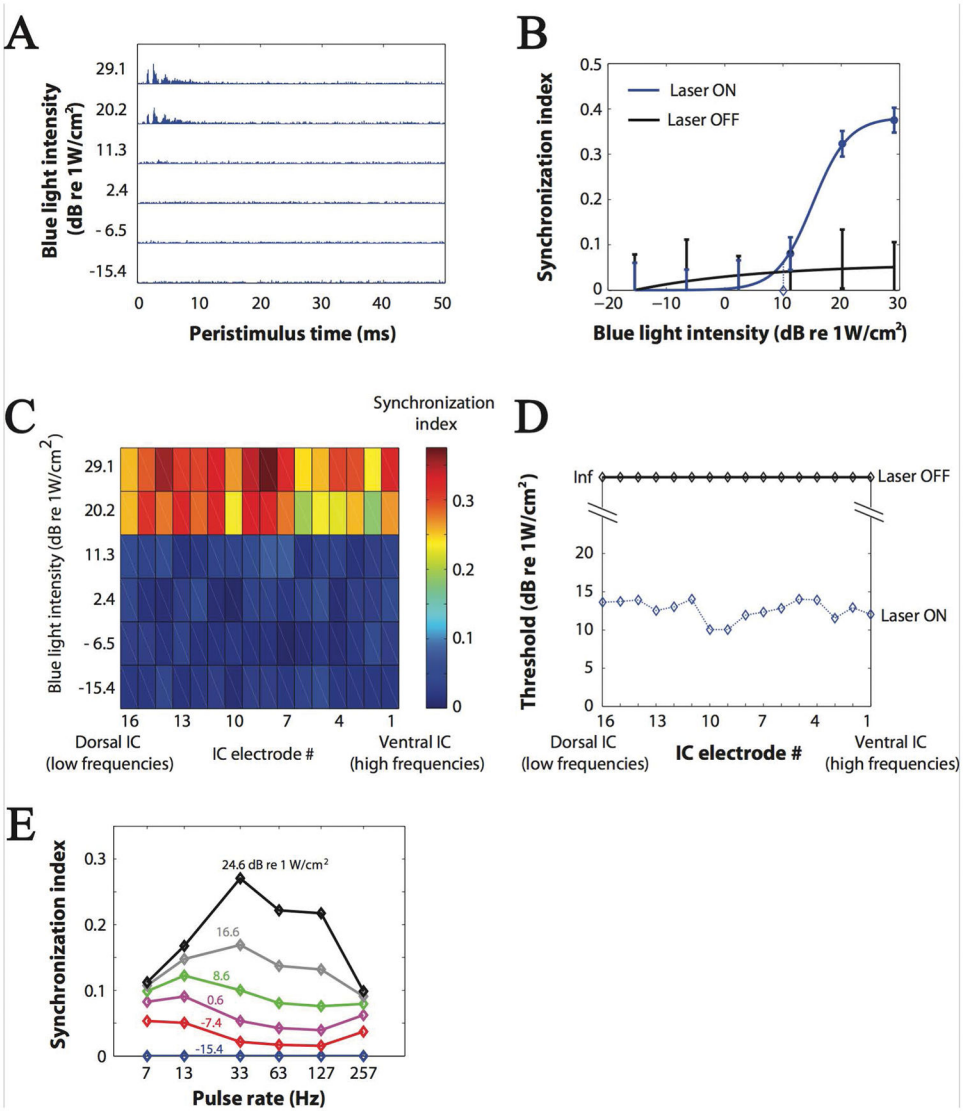

Figure 3.

Analysis of synchronization in IC in ChR2+ cases (A–D: KND 23; E: KND 37). A) A clear response near stimulus onset at the largest stimulus intensities is observed in poststimulus time histograms (5000 bins, electrode #8, 5 Hz pulse rate, 1-ms duration light pulses). B) Synchronization index (SI) in same electrode (blue dots are means, error show ± 2 standard deviations, blue line: sigmoidal fit). The SI threshold was near 10 dB re: 1W/cm^2 (blue diamond) and it approached saturation at 30 dB re: 1W/cm^2. Black points show laser OFF condition. C) SI mapping as a function of intensity for all electrodes. D) Synchronization thresholds as a function of IC electrode. Thresholds were defined as the light intensity at which SI was significant (Rayleigh test, $p<0.01$). E) SI as a function of pulse rate at different light intensities (from electrode #14, with best response to sound frequency of 16 kHz). At the higher light intensities, SI rolls off at pulse rates above 60 Hz.

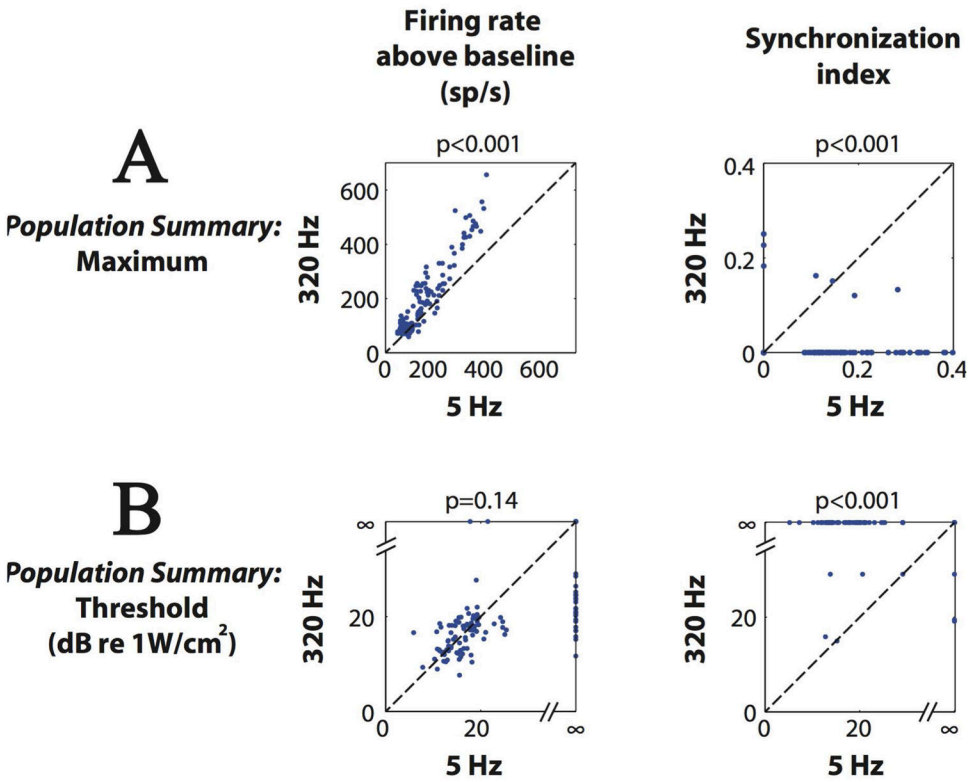

Figure 4.

Summary data (8 mice, 16 electrodes each) for pulse rates of 5 and 320 Hz. A) Maximum firing rate was greater in the 320 Hz condition, consistent with increased stimulation energy ($p<0.001$, Mann-Whitney U-test). In contrast, SI was significantly lower in the 320 Hz condition ($p<0.001$, Mann-Whitney U-test). Non-significant SI were set to 0 to facilitate comparison. B) Firing rate thresholds were not significantly different between the 5 and 320 Hz conditions ($p=0.14$, Mann-Whitney U-test) whereas SI thresholds were significantly lower at the 5 Hz condition ($p<0.001$, Mann-Whitney U-test). In most cases, there was no significant SI at 320 Hz (threshold = ∞) in spite of large firing rate response.

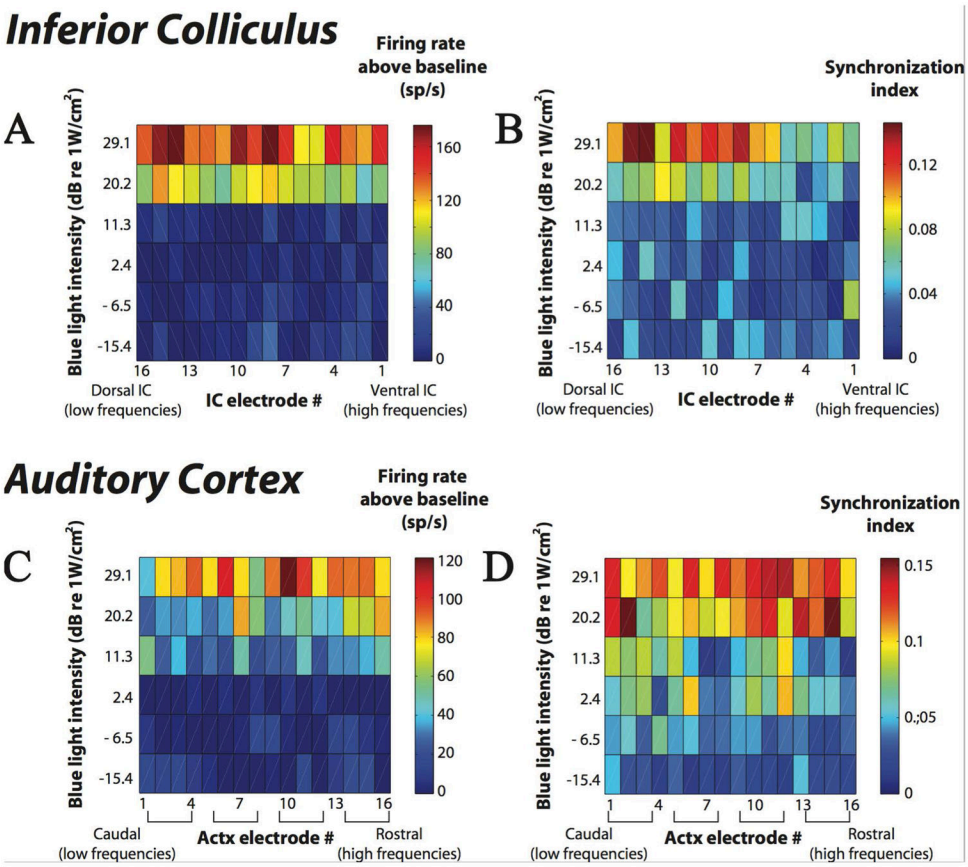

Figure 5.

Optical stimulation activates both the IC and Actx (KND 25). In the IC, average firing rate (A) and SI (B) show broad patterns across electrodes with thresholds in the 10 to 20 dB re: 1W/cm^2 range (1-ms duration light pulse at 5 Hz, 40 presentations). In Actx firing rate (C) and SI (D) also show broad patterns. Brackets indicate the 4×4 electrode set-up of the recording probe: e.g. electrode contacts 1–4 are located within a column of the Actx.

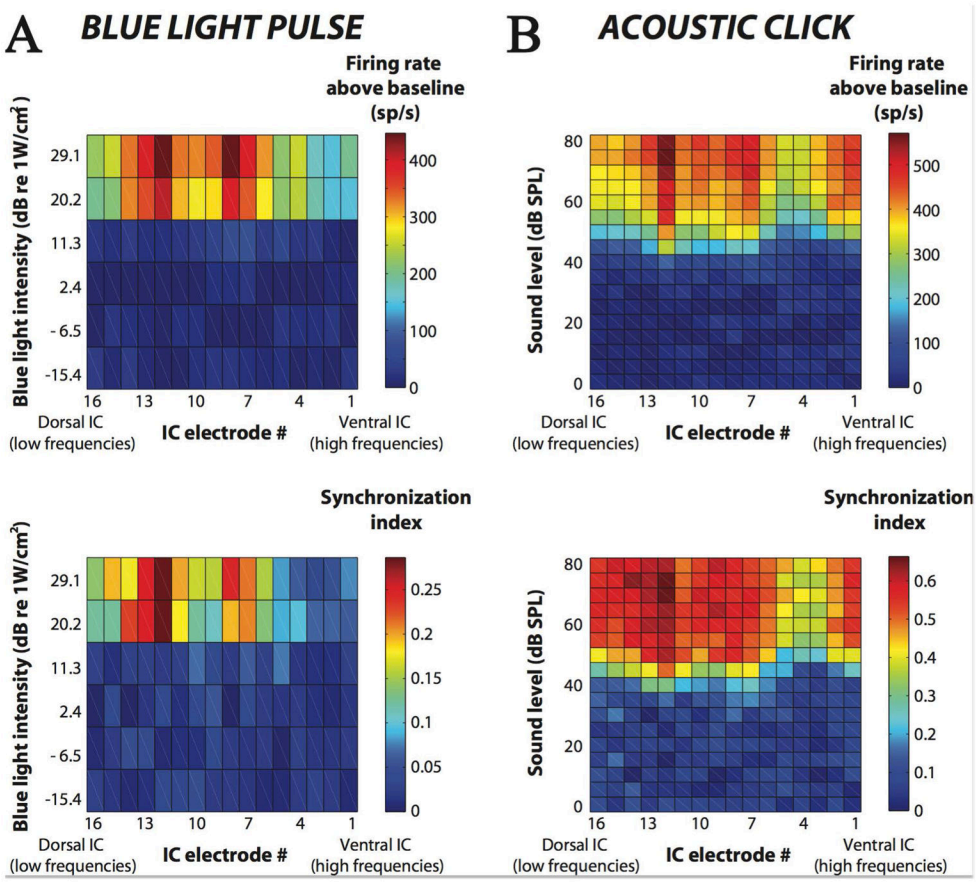

Figure 6.

Comparison of IC responses between optical and acoustic stimulation in a ChR2+ mouse (KND 21). A) Activation maps in response to 1 ms duration blue light pulses presented at a rate of 5 Hz (80 presentations). Top: Average firing rate and bottom: SI both show broad activation with thresholds in the 10 to 20 dB re: 1W/cm^2 range. B) Activation maps in response to 0.1 ms duration acoustic clicks presented at a rate of 23 Hz (80 presentations) for sound levels ranging from 0 to 80 dB SPL. Top: Average firing rate and bottom: SI. Both measures show broad activation with thresholds in the 40 to 60 dB SPL range.

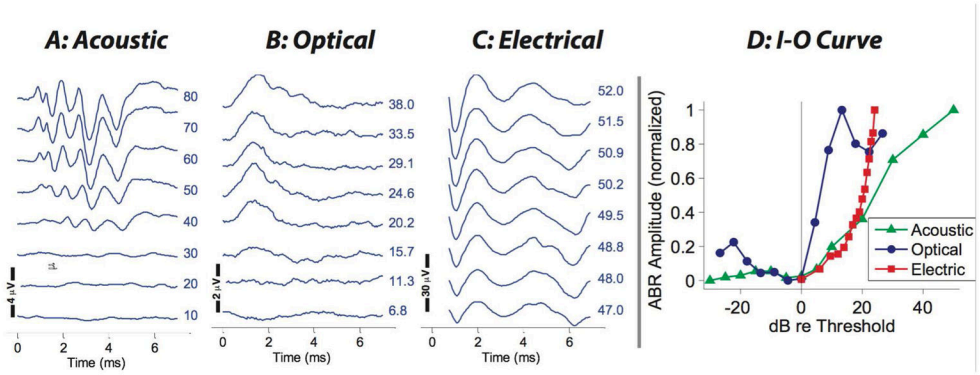

Figure 7.

Acoustic, optical, and electrical evoked potentials (KND 38). A) Waveforms from an acoustically evoked ABR recorded in response to different levels of a 23 Hz 1-ms stimulus (512 repetitions). B) Waveforms of the optically evoked ABR recorded with a 1-ms 23 Hz blue light pulse presented 500 times to the CN. C) Electrically evoked ABR in the same animal with a level series using a 200 μs electrical pulse presented at 27 Hz with 100 repetitions. D) Input-output (I–O) curves showing a roughly similar shape for the three types of stimulation. Normalized baseline to peak output (μV) was used.